https://doi.org/10.5194/acp-2020-757
Preprint. Discussion started: 30 July 2020


# Microphysical Properties of Three Types of Snow Clouds: Implication to Satellite Snowfall Retrievals

Hwayoung Jeoung[1], Guosheng Liu[1], Kwonil Kim[2], Gyuwon Lee[2], and Eun-Kyoung Seo[3]

1. Department of Earth, Ocean and Atmospheric Science, Florida State University, Tallahassee, Florida, U.S.A.
2. Department of Astronomy and Atmospheric Sciences, Center for Atmospheric REmote Sensing (CARE), Kyungpook National University, Daegu 41566, Republic of Korea
3. Department of Earth Science Education, Kongju National University, Kongju 314-701, Republic of Korea

https://doi.org/10.5194/acp-2020-757
Preprint. Discussion started: 30 July 2020


Atmospheric Chemistry and Physics Discussions


Abstract

Ground-based radar and radiometer data observed during the 2017-18 winter were used to simultaneously estimate both cloud liquid water path and snowfall rate for three types of snowing clouds: near-surface, shallow and deep. Surveying all the observed data, it is found that near-surface cloud is the most frequently observed cloud type with an area fraction of over 60%, while deep cloud contributes the most in snowfall volume with about 50% of the total. The probability distributions of snowfall rates are clearly different among the three types of clouds, with vast majority hardly reaching to 0.3 mm $h^{-1}$ (liquid water equivalent snowfall rate) for near-surface, 0.5 mm $h^{-1}$ for shallow, and 1 mm $h^{-1}$ for deep clouds. However, liquid water path in the three types of clouds all has substantial probability to reach 500 g $m^{-2}$. There is no clear correlation found between snowfall rate and liquid water path for any of the cloud types. Based on all observed snow profiles, brightness temperatures at Global Precipitation Measurement Microwave Imager channels are simulated, and the ability of a Bayesian algorithm to retrieve snowfall rate is examined using half the profiles as observations and the other half as *a priori* database. Under idealized scenario, i.e., without considering the uncertainties caused by surface emissivity, ice particle size distribution and particle shape, the study found that the correlation as expressed by $R^2$ between the "retrieved" and "observed" snowfall rates is about 0.33, 0.48 and 0.74, respectively, for near-surface, shallow and deep snowing clouds over land surface; these numbers basically indicate the upper limits capped by cloud natural variability, to which the retrieval skill of a Bayesian retrieval algorithm can reach. A hypothetical retrieval for the same clouds but over ocean is also studied, and a major improvement in skills is found for near-surface clouds with $R^2$ increased from 0.33 to 0.54, while virtually no change in skills is found for deep clouds and only marginal improvement is found for shallow clouds. This study provides a general picture of the microphysical characteristics of the different types of snowing clouds and points out the associated challenges in retrieving their snowfall rate from passive microwave observations.

https://doi.org/10.5194/acp-2020-757
Preprint. Discussion started: 30 July 2020


Atmospheric Chemistry and Physics Discussions

## 1. Introduction

Snowfall is an important component in the global hydrological cycle. Its global distribution may be observed using satellite-based passive and active microwave sensors. Currently, there are multiple satellites in operation carrying passive microwave sensors that are potentially able to be used for snowfall observations, which offers great spatial and temporal coverages for various snowfall related studies. Meanwhile, while only a few spaceborne active sensors are currently available for snowfall observations, they have the advantage of providing information on the vertical structure of precipitation. Nevertheless, whether active or passive sensors are used, in order to convert the observed radiative signatures (brightness temperature or radar reflectivity) to snowfall rate, two factors related to the snowing clouds play an essential role: one is the vertical extent of the cloud layer and the other is the cloud microphysical properties such as particles' phase and amount. Using ground-based observations from multiple sensors, in this study we intend to understand these properties for three distinctive types of snowing clouds. By performing radiative transfer simulations, we further investigate the implication of the variability in microphysical properties to satellite snowfall retrievals from passive microwave observations.

Snowfall retrieval has been investigated recently for both active and passive satellite measurements. The cloud radar onboard CloudSat satellite (Stephens et al., 2002; Tanelli et al., 2008) is the first spaceborne active sensor in operation that is suitable for snowfall observations. It has a minimum detectability of near −30 dBZ near the ground, allowing to observe the weak scattering signal from snowflakes. Kulie et al. (2016) used CloudSat cloud classification and snowfall rate retrievals to partition snowfall observations into shallow cumuliform and deep nimbostratus snowfall categories. Their results show that there are abundant shallow snow cloud cells globally and they can be associated with strong convection and heavy snowfall. For example, they found that shallow snowfall comprises about 36% in the 2006–10 CloudSat snowfall dataset by occurrence, while constituting some 18% of the estimated annual global snowfall accumulation. Shallow precipitation can be easily missed by space-borne radars. Although CloudSat radar provides information on the vertical structure of precipitation, there is a blind zone below

https://doi.org/10.5194/acp-2020-757
Preprint. Discussion started: 30 July 2020




about 1.5 km due to ground clutter contamination. In most analysis, the lowest range bin (bin depth is ~240 m) where radar data are not contaminated by surface clutter is often the third (fifth) above the actual surface over oceanic (land) surfaces (Wood et al., 2013; Kulie and Bennartz, 2009; Liu, 2008a; Marchand et al., 2008). Hudak et al.(2008) studied the ability of CloudSat radar to detect precipitation in cold season clouds using data from a C band weather radar at King City, Ontario. They found that the most frequent cause of a miss in detection by CloudSat radar was due to ground clutter removal of valid echoes by the algorithm. Similarly, Chen et al. (2016) compared snowfall estimates from CloudSat radar (Wood et al., 2013) and ground radar derived Multi-Radar and Multi-Sensor (MRMS) product (Zhang et al., 2016), and found that the lowest height with valid estimate for most (99.41%) snowfall events in CloudSat product is over 1 km above surface, whereas it for 76.41% of the corresponding MRMS observations is below 1 km.

Using satellite passive microwave observations at high frequency channels, snowfall may be retrieved due to the scattering of upwelling radiation by snowflakes (Katsumata et al., 2000; Bennartz and Bauer, 2003; Skofronick-Jackson and Johnson, 2011; Gong and Wu, 2017). Retrieval algorithms have been developed both in research mode (Kim et al., 2008; Kongoli et al., 2015; Liu and Seo, 2013; Noh et al., 2006; Skofronick-Jackson et al., 2004) and for operations (Kummerow et al., 2015; Meng et al., 2017). Skofronick-Jackson et al. (2004) and Kim et al. (2008) developed physically-based retrieval algorithms which seek the best match between radiative transfer model simulated and satellite observed brightness temperatures. The Liu and Seo (2013) and Kongoli et al. (2015) algorithms are mostly statistical in which many pairs of radar and/or gauge-measured snowfall and satellite measured brightness temperatures are used to develop their statistical relations. The Noh et al. (2006) and Kummerow et al. (2015) snowfall algorithms are based on the Bayesian theorem; an *a priori* database linking snowfall and brightness temperatures needs to be prepared before conducting retrievals. The snowfall in the database is often retrieved from radars and the brightness temperatures are either from collocated measurements by passive microwave radiometers or simulated by radiative transfer models. The Meng et al. (2017) algorithm uses a one-dimensional variational method to seek the consistency between measured brightness temperatures and

https://doi.org/10.5194/acp-2020-757
Preprint. Discussion started: 30 July 2020



microphysical properties in the atmospheric column. Its performance has been verified by surface radar and gauge observations over the U.S. with satisfactory results.

Although the above successes have been achieved by previous investigators, there are still large discrepancies among different snowfall retrievals (Casella et al., 2017; Skofronick-Jackson et al., 2017; Tang et al., 2017). Algorithm uncertainty arises from many factors; one of them is the insufficient knowledge of microphysical properties of the snowing clouds, in particular, the amount of cloud liquid water. The increase in brightness temperature over cloudy skies due to liquid water emission in snowing clouds complicates the snowfall detection and retrieval problems (Liu and Curry, 1997; Liu and Seo, 2013; Wang et al., 2013). Wang et al. (2013) showed that the warming by liquid water emission has a similar magnitude to the cooling by ice scattering on microwave brightness temperatures at frequencies higher than 80 GHz. Liu and Seo (2013) discovered a warming rather than cooling signal in high-frequency brightness temperature in most snowfall cases they analyzed.

In addition, correctly simulating brightness temperatures is needed for physical snowfall retrievals as well as data assimilation of radiance observations in numerical weather prediction models. Yin and Liu (2019) has studied the bias characteristics of observed minus simulated brightness temperatures at high frequency channels of Global Precipitation Measurement Microwave Imager (GPM/GMI) under snowfall conditions. In their study, a radiative transfer model that includes single-scattering properties of non-spherical snow particles is used to simulate brightness temperatures at 89 through 183 GHz. The input snow water content profiles are derived from CloudSat radar measurements. The results show that the discrepancy between simulated and observed brightness temperatures is the greatest for very shallow or very deep snowing clouds, although it is generally less than 3 K when averaged over all selected pixels under snowfall conditions. They explained the results as follows. For very shallow snowing clouds, cloud liquid water may be rich and contributes substantially to the observed brightness temperatures, while the radiative transfer model inputs based on CloudSat radar retrievals failed to account for this liquid water abundance. For very deep snowing clouds, they hypothesized that CloudSat radar experiences substantial attenuation as well as non-Rayleigh scattering, which leads to higher simulated brightness temperatures than observed. A better understanding of the microphysical properties in very shallow and very deep snowing clouds is clearly needed to reduce the discrepancies between simulated and observed brightness temperatures.

A field experiment was conducted over the Korean Peninsula during the winter of 2017-2018, coinciding with the 2018 winter Olympic Games (ICE-POP 2018: International Collaborative Experiments for PyeongChang 2018 Olympic and Paralympic Winter Games). During the field experiment, many ground-based observations including radar, radiometer and *in situ* observations were conducted. In this study, we analyze the vertical structure and microphysical properties of these snowing clouds, with focus on their potential impacts on satellite remote sensing of snow precipitation. The main objective of the study is to gain better understanding of the characteristics of snowing clouds that are critical to satellite remote sensing of snowfall.

## 2. Data and Methods

### 2.1 Ground-based Cloud Radar and Radiometer

Observations from the Radiometer Physics GmbH-Frequency Modulated Continuous Wave 94 GHz cloud radar (RPG-FMCW, 2015) are the primary data source for this study. This vertical pointing radar is installed at 37.66°N, 128.70°E (altitude 735 m above sea level) over Korean Peninsula during the ICE-POP 2018 field campaign. It has an operation frequency of 94 GHz for radar backscatter and Doppler spectrum measurement and an embedded 89 GHz passive channel for liquid water path measurement. It is noted that while we refer this instrument as a cloud radar for convenience, it indeed includes an independent passive microwave channel at 89 GHz, which is used for cloud liquid water estimation. There is clearly an advantage of this instrument in studying the composition of cloud liquid and ice over those that measure radar reflectivity and brightness temperature by two separate instruments because this instrument measures emission and scattering signatures from the same cloud volume, therefore, avoids beam mismatching problem by a separated radar and radiometer. The vertical resolution of radar reflectivity measurement is selectable from 1, 5, 10, or 30 m, with overall radar calibration accuracy better than 0.4 dB. The minimum detectable radar reflectivity depends on the range and vertical resolution; at its typical operation mode of 30 m resolution, it is -36 dBZ at 10 km height, which is

https://doi.org/10.5194/acp-2020-757
Preprint. Discussion started: 30 July 2020



sufficiently sensitive for snowfall detection. In addition to radar reflectivity, the RPG-FMCW also measures Doppler spectrum with a Doppler velocity resolution of 1.5 cm $s^{-1}$.

## 2.2 Retrieved Microphysical Variables

In this study, the radar reflectivity $Z_e$ is converted to snow water content (SWC) and snowfall rate (S) using the $Z_e$-SWC relation of Yin and Liu (2017) and Ze-S relation of Liu (2008a). The Yin and Liu's $Z_e$-SWC relation is given by

$$SWC = 0.024 Z_e^{0.75}, \quad (1)$$

where SWC is in g $m^{-3}$ and $Z_e$ is in $mm^6$ $m^{-3}$. In developing the above equation, three snow particle types are employed: sectors, dendrites (Liu, 2008b), and oblate aggregates (Honeyager et al., 2016). The backscatter cross sections of the three snowflake types are computed using discrete dipole approximation (DDA) (Draine and Flatau, 1994; Liu, 2004). The Liu's S-$Z_e$ relation is given by

$$Z_e = 11.5 S^{1.25}, \quad (2)$$

where S is in mm $h^{-1}$ (liquid water equivalent snowfall rate) and $Z_e$ is in $mm^6$ $m^{-3}$. The backscatter cross sections in the Liu (2008b) relation are computed for rosettes, sectors and dendrites using DDA.

In addition to radar reflectivity, the mean Doppler velocity and spectral width, the RPG-FMCW also measures brightness temperature at 89 GHz. While there is a liquid water path (LWP) variable produced by the manufacture-provided software, details about the liquid water path retrieval algorithm and its accuracy have not been well documented. In this study, we chose to adapt the algorithm of Liu and Takeda (1988) in computing liquid water path from 89 GHz brightness temperatures. Briefly, the brightness temperature $T_B$ received by an up-looking radiometer can be divided into three portions, i.e., clear-sky emission, liquid cloud water emission, and upward emission from the surface and the atmosphere below cloud but being scattered back by the cloud. The emissivity of the liquid water cloud $\varepsilon_c$ may then be approximated by

$$\varepsilon_c = \frac{T_a(T_B - T_{Ba})}{T_c(T_a - T_{Ba})}, \quad (3)$$

where $T_a$ is a radiatively-mean temperature of the atmosphere in Kelvin, which can be evaluated by absorption-coefficient-weighted averaging atmospheric temperatures in vertical. Its value roughly equals to the temperature around 1.5 km altitude. $T_c$ is the mean temperature of the cloud layer. $T_{Ba}$ is the brightness temperature from the liquid-free atmosphere, which is derived using interpolation between measured $T_B$s at echo-free regions in this study. From $\varepsilon_c$ calculated from (3), liquid water path (LWP) can be derived by

$$\mathrm{LWP} = \frac{\lambda \rho_L}{6\pi \Im\left\{\frac{m^2-1}{m^2+2}\right\}} ln\,(1-\varepsilon_c)\,, \tag{4}$$

where $m$ is the refractive index of water at temperature $T_c$, $\lambda$ is wavelength, $\rho_L$ is liquid water density (1000 kg m$^{-3}$) and $\Im\{\,\}$ indicates taking the imaginary part.

In Fig.1 shown is an example of the liquid water path retrieved in this study together with radar reflectivity cross sections and liquid water path retrieval from the manufacture-provided algorithm. It is seen that in clear-sky regions our liquid water path retrievals are close to zero, while the manufacture-provided retrievals have a positive bias of about 30 g m$^{-2}$. In cloudy regions, the two liquid water path values compare much closer to each other. Based on this comparison, we believe that the liquid water path values retrieved in this study are more reasonable. Therefore, our retrievals will be used in the following analysis.

## 2.3 Snowing Cloud Detection

All snow events have been identified from the RPG-FMCW observations during 1 November 2017 through 30 April 2018 (6 months). To separate snow and rain at surface, the scheme of Sims and Liu (2015) is implemented. In their study, the effects of multiple geophysical parameters on precipitation phase were investigated using global ground-based observations over multiple years. They showed that wet-bulb temperature is a key parameter for separating solid and liquid precipitation and the low-level temperature lapse rate also affects the precipitation phase. Geophysical parameters from the Modern Era Reanalysis for Research and Applications Version-2 (MERRA-2) (Gelaro et al., 2017) were used in this study as input to the Sims and Liu scheme. In addition, we use the near-surface reflectivity higher than -20 dBZ as the criteria for snowfall detection; all radar data

https://doi.org/10.5194/acp-2020-757
Preprint. Discussion started: 30 July 2020




analyzed for snowing clouds in the following sections have a near-surface radar reflectivity greater than -20 dBZ.

Cloud top height is used for the determination of cloud types. As shown in Fig.2, radar reflectivity above cloud top is often noisy as shown between 11 and 16 UTC. Therefore, it is often problematic to determine cloud top height by simply using a radar reflectivity threshold. However, we found that Doppler spectral width is a reliable indicator to identify clouds as shown in the bottom panel in Fig.2. Using visual examination, we found that Doppler spectral width commonly reduces to less than 0.1 m $s^{-1}$ above cloud top. In Fig. 2, we show in the upper panel the cloud top height in the black solid line as determined by the criteria of the spectral width >0.1 m $s^{-1}$ for snowing clouds with near-surface radar reflectivity greater than –20 dBZ. It appears that the criteria well capture the cloud tops.

## 2.4 Other Ancillary Data

While quantitative analysis was not conducted, data collected at the same location by PARticle SIze VELocity (PARSIVEL; Löffler-Mang and Joss, 2000; Battaglia et al., 2010; Tokay et al., 2014), 2-Dimensional Video Distrometer (2DVD; Kruger and Krajewski, 2002), and Multi-Angle Snowflake Camera (MASC; Garrett et al., 2012; Grazioli et al., 2017) are used for confirmation of precipitation phase and particle types. A PARSIVEL is an optical disdrometer which uses a 54 $cm^2$ laser beam in the wavelength of 650 nm. It measures the size and fall velocity of individual precipitation particles with diameter ranging from 0.2 mm to 25 mm for solid particles. An autonomous PARSIVEL unit (Chen et al., 2017) from NASA was collocated with the RPG-FMCW cloud radar during the field campaign. A collocated 2DVD provides detailed information on size, fall velocity, and shape of individual hydrometeors with two orthogonal fast line-scan cameras. The camera provides images of particles which are matched for individual particles. The matched individual particles are then corrected for shape distortion. In addition, detail images of particles are provided from MASC that is composed of three cameras separated horizontally by an angle of 36 degrees and simultaneously takes high-resolution (35 μm per pixel) photographs of free-falling hydrometeors. Hydrometeor classification algorithm based on the supervised machine learning technique (Praz et al., 2017) is applied to the

https://doi.org/10.5194/acp-2020-757
Preprint. Discussion started: 30 July 2020



individual images of particles. This procedure identified the precipitation type (small particles, columnar crystals, planer crystals, combination of columnar and plate crystals, aggregates, and graupel) and the degree of riming.

## 2.5 Dividing Snowing Clouds to Three Types

The winter weather at the observational site is largely influenced by passing storms associated with low-pressure frontal systems. A common radar reflectivity cross section is similar to that shown in Fig.1 where deeper clouds lead to shallower convective cells. The deeper clouds are related to the low-pressure system crossing the Korean peninsula or passing its south and the shallower clouds are linked to air-sea interaction under the control of a high-pressure cold air system after front passing. In consideration of the implications to satellite snowfall remote sensing, we group the snowing clouds into three types: deep, shallow and near-surface. The "deep" snowing clouds are those with cloud top higher than 4 km, which are considered to be easily detected by both space-borne radars and radiometers at high microwave frequencies. They are mostly generated by large-scale lifting of frontal systems. We define the "shallow" snowing clouds as those with cloud top between 1.5 and 4 km. Large part of the snowing clouds in this group are associated with convective cells in unstable airmasses after the passing of fronts. These are the group that space-radars and radiometers may sometimes have difficulties to detect because of their shallowness and liquid-water rich. The "near-surface" group is defined as those having cloud top lower than 1.5 km. Because of their shallowness, this group of snowing clouds will likely be hidden within ground-clutters for space-radars. Ground-based observations have the advantage to detect them from bottom up.

In Fig.1, examples are shown for the three snowing cloud types, together with liquid water path retrieved from RPG-FMCW observations using algorithms described in section 2.2. In this case, the largest value of liquid water path was seen in the transition from shallow to near-surface snowing clouds near 12 UTC, while the strongest radar reflectivity values (i.e., the heaviest snowfall) occurred in the deep snowing cloud between 01 to 05 UTC on 24 December.

Surveying all observed data for the entire winter, the relative frequencies of occurrence (area fraction) and snowfall amount (volume fraction) for the three types of

https://doi.org/10.5194/acp-2020-757
Preprint. Discussion started: 30 July 2020



snowing clouds are shown in Fig.3. As described earlier, we used -20 dBZ at the lowest bin to identify snow events. The snowfall volume is the accumulated snowfall with the rate estimated by eq.(2) from radar reflectivity at the lowest bin. Over half (67.4%) of the observed samples are near-surface snowfall, followed by shallow (21.2%) and then deep (11.4%) snowing clouds. However, deep snowing clouds contribute the most to the total snowfall volume (45.3%), followed by shallow (28.5%) and then near-surface (26.2%) snowing clouds.

## 3. Microphysical Properties of Snowing Clouds

### 3.1 Case Examples

(a) Deep and "dry" followed by near-surface snowing clouds

From 7 to 8 March 2018, a low-pressure system passed the south of the Korea Peninsula, and solid precipitation was observed at the radar site from 09 UTC on the 7$^{th}$ through 24 UTC on the 8$^{th}$. In Fig.4 shown are cross section of radar reflectivity and time variation of liquid water path and snow water path (SWP, vertically integrated snow water content). Surface PARSIVEL and 2DVD observations indicated that snow particle types are mostly snowflakes from 09 UTC on the 7$^{th}$ to 06 UTC on the 8$^{th}$, while rimed ice particles and graupels are also observed then after. The radar and radiometer observations indicate that the deep clouds have cloud top higher than 8 km and peak snow water path value about 400 g m$^{-2}$. However, liquid water in the deep clouds is low, with liquid water path constantly below 150 g m$^{-2}$. Once the deep clouds pass the station, the clouds became much shallower, mostly being classified as near-surface snowing clouds. However, their liquid water path increased substantially with peak values close to 600 g m$^{-2}$, which is consistent with the observed rimed ice particles and graupels during this period.

(b) Deep and "wet" followed by shallow snowing clouds

On 28 February 2018, deep snowing clouds associated with a low-pressure system were observed at the radar site, followed by shallow snowing clouds that lasted till 03 UTC on March 1. Radar reflectivity, liquid water path and snow water path are shown in Fig.5.

https://doi.org/10.5194/acp-2020-757
Preprint. Discussion started: 30 July 2020



Surface PARSIVEL observations indicated melting snow before 04 UTC on February 28, which may have contributed the liquid water path peak around 04 UTC. Heavy snowfall was observed from 04 to 14 UTC on 28 February. Liquid water path was high for both the deep and shallow clouds with peaks higher than 400 g m$^{-2}$ even without including the portion of melting snow before 04 UTC on the 28$^{th}$. Rimed snow particles were observed at surface corresponding to the shallow snow cell based on 2DVD and MASC data.

## 3.2 Liquid versus Ice in Snowing Clouds

During the 6-month period, a total of 374 hours of snow precipitation have been observed by the RPG-FMCW. The frequency distributions of 5-minute averaged surface snowfall rate and liquid water path are shown in Fig.6 with both surface snowfall rate and liquid water path in logarithm scale. On average, deeper clouds generate heavier snowfall; near-surface and shallow snowing clouds produce snowfall rarely heavier than 0.5 mm h$^{-1}$, while snowfall rate in deep snowing clouds reaches over 1 mm h$^{-1}$. Higher values of cloud liquid water path are also more likely observed in deeper clouds. However, the likelihood of a substantial amount of liquid water in shallower clouds is also high. For example, for the liquid water path range of 100~250 g m$^{-2}$ the frequency values are still reaching about 10% for near-surface and shallow snowing clouds. On the upper limit, liquid water path in all clouds only occasionally exceeds 500 g m$^{-2}$.

In Fig.7, we show the scatterplot of surface snowfall rate versus liquid water path averaged over a 5-minute period. As indicated in case studies earlier, the two variables hardly vary in a correlated fashion, neither positively nor negatively. For deep snowing clouds, the heaviest snowfall corresponds to a liquid water path of about 200 g m$^{-2}$, while further increasing in liquid water path does not seem to enhance surface snowfall. For shallow and near-surface snowing clouds, the snowfall rate is confined between 0 to 0.6 mm h$^{-1}$ while liquid water path stretches from 0 to 600 g m$^{-2}$ without coherent variation between liquid water path and surface snowfall rate. Additionally, unlike heavy snowfall preferably occurring in deep snowing clouds, large values of liquid water path (say > 300 g m$^{-2}$) are almost equally probable to be found in near-surface, shallow and in deep snowing clouds.

https://doi.org/10.5194/acp-2020-757
Preprint. Discussion started: 30 July 2020




The mean state and its variability of cloud liquid water are also examined in the 2-dimensional space of near surface radar reflectivity and cloud top height, as shown in Fig.8. In this figure, the mean values of (a) the number of occurrences, (b) liquid water path, and (c) standard deviation of liquid water path in each 2 dBZ by 500 m grid are shown based on the 5-minute averaged data. The number of occurrences diagram indicates that heavier snowfall (stronger radar reflectivity) tends to have a higher cloud top for cases with near surface radar reflectivity greater than 0 dBZ although this tendency is not clear for cases with lower values of near surface radar reflectivity. On average, the higher values of liquid water path are along the right-most edge of the data-covered area in the plot, indicating that given the same surface snowfall rate clouds with the lowest top height tend to contain the highest amount of liquid water. The variability of liquid water path as expressed by its standard deviation further indicates that liquid water path in clouds with lower top heights is more variable in magnitude as well.

To express the "dryness" of the snowing clouds, one may use the glaciation ratio (GR) defined as (Liu and Takeda, 1988):

$$GR = \frac{SWP}{LWP+SWP} \times 100\% . \quad (5)$$

The GR parameter indicates the fraction of total condensed water in the column that has been converted to solid phase. In Fig.9, we show how the GR values are related to (a) cloud top height, (b) surface snowfall rate and (c) cloud mean temperature (temperature at the geometrical middle of a reflectivity profile). Generally speaking, clouds with higher tops, associated with higher snowfall rate or with colder mean temperature tend to have higher degrees of glaciation, although the scatters are extremely large. For example, for a shallow snowing cloud with 0.2 mm $h^{-1}$ snowfall rate, its glaciation ratio can be any value from near 0 to about 100%, probably depending on the development stage of individual cells. Corresponding to the clouds with their heaviest snowfall rate, deep snowing clouds have a glaciation ratio of about 60% while shallow and near-surface snowing clouds only have their glaciation ratio less than 20%, which adds extra difficulties for detecting snow in these types of clouds by passive microwave observations. There is loosely a trend that clouds

https://doi.org/10.5194/acp-2020-757
Preprint. Discussion started: 30 July 2020



with a lower mean temperature have a higher degree of glaciation. For near-surface snowing clouds, this trend is less clear with their glaciation degree hardly over 50%.

### 3.3 Vertical Structures

The mean vertical structure of the snowing clouds may be expressed by contoured frequency by altitude diagrams (CFADs; Yuter and Houze, 1995) of (a) radar reflectivity, (b) mean Doppler velocity, and (c) Doppler spectral width, as shown in Fig. 10. For deep snowing clouds, the radar reflectivity CFADs show a relatively narrow spread with a sharp radar reflectivity decreases with the increase of altitude above 3 km ("left-tilting" structure), implying that most of the precipitation growth occurs above 3 km. For shallow clouds, the "left-tilting" structure starts from near surface and the frequency has broader distribution at each level. In contrast, the near-surface snowing clouds do not show such "left-tilting" structure, but rather have a broad distribution below their cloud top height, indicating that the precipitation maximum does not necessarily situate near the surface in these profiles. We interpret that the broad distribution of frequencies at each level is likely due to the convective nature of these clouds, so that the precipitation profile is largely determined by the development stage of the clouds. For example, developing clouds have their precipitation maximum in the upper portion while matured clouds have their precipitation maximum in the lower portion in the vertical profiles.

For mean Doppler velocity, the most likely values are around -1 m $s^{-1}$ (the negative sign indicates downward movement), corresponding to the terminal velocity of unrimed to moderately rimed aggregates (Locatelli and Hobbs, 1974). There is a tendency that particles in upper levels fall somewhat slower than those in the lower levels. The Doppler spectral width indicates that particles in the upper levels have a narrower spectrum. Combining the vertical profiles of mean Doppler velocity and spectral width, it is concluded that ice particles at upper levels have a narrower size distribution and lower terminal velocity.

## 4. Implications to Passive Microwave Remote Sensing

https://doi.org/10.5194/acp-2020-757
Preprint. Discussion started: 30 July 2020




To understand how the microphysical properties in snowing clouds impact on passive microwave remote sensing, a radiative transfer model simulation at GPM/GMI channels has been conducted using the measured liquid and snow water quantities as a guidance for the model input. The radiative transfer model developed by Liu (1998) has been used in this simulation, which uses a four-stream discrete ordinates method to solve the radiative transfer equation. For snow particles, the single-scattering properties calculated by discrete dipole approximation for sector type snowflakes (Liu, 2008b) are used. Based on studies of Geer and Baordo (2014), the single-scattering properties for the sector type snowflakes work reasonably well in radiative transfer simulations for middle latitude snowstorms. Since the emphasis of this study is to assess the impact of cloud microphysics on satellite remote sensing, the variability of surface emissivity is not considered. In all the following simulations, we assign an emissivity of 0.9 for land surface for all GMI channels and a 5 m $s^{-1}$ wind speed over ocean to compute surface emissivity.

### 4.1 Masking Effect to Scattering Signatures by Cloud Liquid Water

Based on analysis shown in section 3.2, liquid water path frequently varies from 0 to 500 g $m^{-2}$ for any of the 3 types of snowing clouds while snowfall rate at surface commonly reaches to 0.3, 0.5, and 1.0 mm $h^{-1}$, respectively, for near-surface, shallow, and deep clouds. We examine how the cloud liquid would mask the ice scattering at two GMI frequencies, 89 and 166 GHz, at viewing angles of 53° for 89 GHz and 49° for 166 GHz using radiative transfer calculations. Using clear-sky brightness temperature $T_{B0}$ as the base, Figure 11 shows how brightness temperature varies as liquid water path and surface snowfall rate increase. Note that in these calculations, we used the observed snowfall rate profiles derived for each cloud type and averaged for various snowfall rate bins. A 1-km deep liquid cloud layer is placed at 0.5-1.5 km, 2.5-3.5 km and 4.5-5.5 km, respectively, for near-surface, shallow, and deep clouds. The liquid water path is increased from 0 to 500 g $m^{-2}$.

For near-surface snowing clouds, the decrease of brightness temperature due to ice scattering is very limited for either 89 or 166 GHz, only a few Kelvin occurring when liquid water path is very low. Therefore, most likely this type of clouds displays a warming signature in the passive microwave observations due to the existence of liquid water clouds.

https://doi.org/10.5194/acp-2020-757
Preprint. Discussion started: 30 July 2020




For shallow snowing clouds, the modeling results show there is still a mostly warming at 89 GHz and an equal mix of warming and cooling at 166 GHz. The masking effect still remains quite significant at 89 GHz even for deep snowing clouds; it can cause an increase in brightness temperature by more than 5 K from clear-sky value. The dominant scattering signature shows at 166 GHz for deep clouds. At surface snowfall rate of 1 mm $h^{-1}$, brightness temperature can decrease from clear-sky value by more than 30 K (color bar only shows up to -15 K) when liquid water path is lower than 100 g $m^{-2}$.

Based on the above modeling results, it is clear that if only relying on scattering signature, i.e., brightness temperature depression, an algorithm will totally fail in retrieving snowfall rate for near-surface clouds and partially fail for shallow clouds. The only cloud type that may have reliable retrievals is the deep snowing cloud. Therefore, a more plausible approach to the retrieval problem is to use a statistical method in which the algorithm utilizes any regularities naturally existing between cloud liquid and snow profiles to search for the most likely snowfall rate. One such approach is the Bayesian retrieval algorithm (Kummerow et al., 1996; Olson et al., 1996; Seo and Liu, 2005). This approach requires that the *a priori* database used in the retrieval has the same characteristics in both microphysical properties and occurring frequency as those in natural clouds.

## 4.2 A Bayesian Retrieval Exercise

In this section, an idealized experiment is designed to examine how a Bayesian retrieval algorithm would perform for the three types of snowing clouds if we only take into account the error caused by the variability of liquid water path and snowfall rate profiles. In other words, we examine how well a Bayesian retrieval algorithm would perform, when assuming no variations in surface emissivity, snowflakes being a fixed type, and particle size distribution following an exponential form. Therefore, this exercise mainly assesses the problems caused by the uncertainties associated with cloud liquid and snow amounts.

First, a total of 18752 5-minute averaged snow profiles are constructed from the 6 months long surface radar observations (including zero snowfall profiles). Each of the snow profile is accompanied with a liquid water path which is assigned to be a 1 km deep layer at 0.5-1.5 km, 2.5-3.5 km and 4.5-5.5 km, respectively, for near-surface, shallow, and

https://doi.org/10.5194/acp-2020-757
Preprint. Discussion started: 30 July 2020




deep clouds. Atmospheric temperature, pressure, and relative humidity profiles are also assigned to these profiles by interpolating MERRA-2 data spatially and temporally to the individual snow profiles. A radiative transfer model calculation is then performed to generate brightness temperatures at 11 GMI channels (all except the 10.7 GHz GMI channels) using the above profiles as input. The 10.7 GHz channel is not considered here because its brightness temperature is merely sensible to either liquid or ice hydrometeors and its GMI channel has too large a footprint size compared to other channels. It is also assumed that surface skin temperature is the same as surface air temperature and surface emissivity is a constant (0.9 for land) for all channels. A sector type snowflake (Liu, 2008b) and an exponential particle size distribution (Sekhon and Srivastava, 1971) are used for all the cases. We then randomly divided the 18752 profiles and their computed brightness temperatures into two equal-number groups; one is used as the *a priori* database for the Bayesian retrieval algorithm, and the other as "observations" to test how well the surface snowfall rate can be retrieved from the "measured" brightness temperatures. To mimic a possible random error in the measured brightness temperatures, a random noise with a maximum magnitude of 1 K is added to the "measured" brightness temperatures before retrieval is performed. A detailed description of the Bayesian retrieval method can be found in Seo and Liu (2005).

In Fig.12 shown are the scatterplots of "measured" versus retrieved surface snowfall rate, separated by snow cloud types. The correction as indicated by $R^2$ (square of linear correlation coefficient) is shown in each diagram. There is virtually no bias between the "measured" and retrieved values. The color of the points in the figures indicates the value of liquid water path associated with individual profiles. Clearly, as the cloud layer deepens, the skill of the retrieval improves. The values of $R^2$ increases from 0.33 for near-surface clouds, to 0.48 for shallow clouds, and to 0.74 for deep clouds. That is, the retrievals can resolve one-third, one-half and three-fourths of the variances in snowfall rate observations for near-surface, shallow and deep clouds, respectively. Another observation from the plots is that departure of points from the one-to-one line does not seem to relate to the magnitude of liquid water path, which implies that it is the randomness in the combination of liquid water path and snowfall rate that is reducing the algorithm's skill, rather than the magnitude of liquid water path itself.

https://doi.org/10.5194/acp-2020-757
Preprint. Discussion started: 30 July 2020



A question one may naturally want to ask is: Will the retrieval skill be improved if the same clouds were moved to areas over ocean where liquid water information is distinguishable at some microwave channels (e.g., 89 GHz)? To answer this question, we perform the same retrieval exercise as mentioned above but assuming the clouds are over an ocean surface with a constant surface wind speed of 5 m $s^{-1}$. Similarly, half of the 18752 samples are used as a priori database and half as "observations". The retrieval results are shown in Fig.13. For deep snowing clouds, the $R^2$ statistic indicates virtually no difference in retrieval skills between over land and over ocean cases, although a visual inspection of the scatterplot shows that a better correspondence between "measured" and retrieved values at snowfall rates lower than 0.2 mm $h^{-1}$. The improvement in retrieval skills for over ocean shallow clouds is marginal with $R^2$ of 0.54 versus 0.48 over land. The most significant improvement in retrieval skills occurs for over ocean near-surface snowing clouds, in which $R^2$ increases from 0.33 over land to 0.54 over ocean. Note that land surface emissivity and ocean surface wind are fixed in the retrieval exercises. Therefore, the improvement is not due to a better knowledge of surface conditions, but rather due to the richer information content on cloud microphysics contained in "measured" brightness temperatures over ocean. One such piece of information must have come from the brightness temperature difference between two polarizations over ocean, which remines mostly zero over land surfaces. The results shown in Fig.13 indicate that the extra polarization information helps the most for retrieving snowfall in near-surface clouds.

To understand the information conveyed in polarization difference of brightness temperatures, we performed a similar simulation to that described in Section 4.1, but replaced land surface to ocean surface with a wind speed of 5 m $s^{-1}$. The changes of depolarization as liquid water path and snowfall rate increase are shown in Fig.14 for each of the 3 cloud types at 89 and 166 GHz. Depolarization is defined as $\Delta T_B = T_{BV} - T_{BH}$, where $T_{BV}$ and $T_{BH}$ are brightness temperatures at vertical and horizontal polarizations, respectively. The change is relative to clear-sky values, $\Delta T_{B0}$. The change in depolarization at 89 GHz is well corresponding to the change in liquid water path, without much dependence on snowfall rate, particularly for near-surface and shallow snowing clouds. Therefore, it is plausible that the increased retrieval skill over ocean for near-surface and shallow clouds is due to the added information on liquid water contained in the polarization

https://doi.org/10.5194/acp-2020-757
Preprint. Discussion started: 30 July 2020


differences. Comparing Figs.12 and 13, it seems that the added information is particularly helpful in improving retrievals at low snowfall rates.

## 5. Conclusions

During the 2017-18 winter season, a ground-based radar and radiometer observation has been carried out over Korean Peninsula as part of the ICE-POP 2018 campaign. Using the coincident radar and radiometer data, we were able to retrieve cloud liquid water path, snow water content and snowfall rate. These microphysical properties and their relation to cloud top height are analyzed in an effort to better understand their implications to satellite remote sensing of snowfall. In the analysis, we divide the approximately 374 hours of observed snowing clouds into near-surface, shallow and deep types, for which the cloud top height is below 1.5 km, between 1.5 and 4 km and above 4 km, respectively. The near-surface snowing clouds are most likely to be missed by currently available space-borne radars because of the blind zone caused by the contamination of surface clutter, and their shallowness and liquid water abundance may also present challenges to satellite radiometer observations. The shallow snowing clouds commonly occur in unstable air mass after the passing of a cold front. It can be detected by space-borne radars with sufficient low minimum detectable radar reflectivity, but the mixture of cloud liquid emission and ice scattering complicates the retrievals by passive microwave observations. The deep snowing clouds are mostly located near frontal zones and low-pressure centers; their strong ice scattering signature makes it the most favorable type among the three for snowfall retrievals by both satellite radars and radiometers. Surveying all the observed data, it is found that near-surface snowing cloud is the most frequently observed cloud type with a frequency of occurrence over 60%, while deep snowing cloud contributes the most in snowfall volume with about 50% of the total snowfall amount.

The probability distributions of surface snowfall rates are clearly different among the three types of snowing clouds, with vast majority of it hardly reaching to 0.3 mm h$^{-1}$

for near-surface, 0.5 mm $h^{-1}$ for shallow, and 1 mm $h^{-1}$ for deep snowing clouds. However, liquid water path in the three types of snowing clouds all has substantial likelihood to be between 0 to 500 g $m^{-2}$, although deeper clouds are somewhat more likely with more liquid water as well. There is no clear correlation, either positive or negative, between surface snowfall rate and liquid water path. However, given the same surface snowfall rate, clouds with lower cloud top height tend to have higher liquid water path. The glaciation ratio defined by the ice fraction in the total condensed water in an atmospheric column is estimated and found to be related to cloud top height, surface snowfall rate and cloud mean temperature, although the relations are very scattered. A higher value of glaciation ratio is generally corresponding to a higher cloud top, a higher surface snowfall rate and lower cloud mean temperature.

Using the approximately 19,000 observed snow cloud profiles, brightness temperatures at GPM/GMI channels are computed, and the ability of a Bayesian type algorithm to retrieve surface snowfall is examined using half the profiles as observations and half as *a priori* database. Under idealized scenario, i.e., without considering the uncertainties caused by surface emissivity, ice particle size distribution and particle shape, the examination results indicate that the correlation as expressed by $R^2$ between the "retrieved" versus "measured" snowfall rates is about 0.33, 0.48 and 0.74, respectively, for near-surface, shallow and deep snowing clouds over land surface. Since this is an extremely idealized retrieval exercise only dealing with the complicated mixture of cloud liquid and snow profiles, these numbers basically indicate the upper limits of how a retrieval algorithm can perform for these snowing clouds. The result also implies that it is the randomness in the combination of liquid water path and snowfall rate that is limiting the algorithm's skill, rather than the magnitude of liquid water path itself. A hypothetical retrieval for the same clouds but over ocean is also studied, and a major improvement in skill for near-surface clouds is found with $R^2$ increased from 0.33 to 0.54, while virtually no change in skill is found for deep clouds and only marginal improvement is found for shallow clouds. The improvement seen in near-surface clouds is interpreted as that some liquid water information is resolved by the polarization difference contained in the over-ocean brightness temperatures. This information helps the most for the otherwise information-poor observations for the near-surface clouds.

By analyzing the radar and radiometer data from one-winter-long observations and the results of a Bayesian retrieval dry run, this study gives a general picture of the characteristics of the different types of snowing clouds and points out the fundamental challenges in retrieving their snowfall rate from passive microwave observations. It is hopeful that these results can help developers improve physical assumptions in future algorithms as well as data users better interpret satellite retrieved snowfall products.

**Acknowledgements.** This research has been supported by NASA under grants 80NSSC19K0718 and NNX16AP27G. Participation of KK and GWL has been supported by the Korea Meteorological Administration Research and Development Program under Grant KMI2018-06810, and by the Korea Environmental Industry & Technology Institute (KEITI) of the Korea Ministry of Environment (MOE) as "Advanced Water Management Research Program" (79615). The authors are greatly appreciative to the participants of the World Weather Research Programme Research Development Project and Forecast Demonstration Project, International Collaborative Experiments for Pyeongchang 2018 Olympic and Paralympic winter games (ICE-POP 2018), hosted by the Korea Meteorological Administration.

## References

Battaglia, A., Rustemeier, E., Tokay, A., Blahak, U. and Simmer, C.: PARSIVEL snow observations: A critical assessment, J. Atmos. Ocean. Technol., doi:10.1175/2009JTECHA1332.1, 2010.

Bennartz, R. and Bauer, P.: Sensitivity of microwave radiances at 85-183 GHz to precipitating ice particles, Radio Sci., 38(4), n/a-n/a, doi:10.1029/2002rs002626, 2003.

Casella, D., Panegrossi, G., Sanò, P., Marra, A. C., Dietrich, S., Johnson, B. T. and Kulie, M. S.: Evaluation of the GPM-DPR snowfall detection capability: Comparison with CloudSat-CPR, Atmos. Res., 197, 64–75, doi:10.1016/j.atmosres.2017.06.018, 2017.

https://doi.org/10.5194/acp-2020-757
Preprint. Discussion started: 30 July 2020



Chen, H., Chandrasekar, V. and Bechini, R.: An improved dual-polarization radar rainfall algorithm (DROPS2.0): Application in NASA IFloodS field campaign, J. Hydrometeorol., doi:10.1175/JHM-D-16-0124.1, 2017.

Chen, S., Hong, Y., Kulie, M., Behrangi, A., Stepanian, P. M., Cao, Q., You, Y., Zhang, J., Hu, J. and Zhang, X.: Comparison of snowfall estimates from the NASA CloudSat Cloud Profiling Radar and NOAA/NSSL Multi-Radar Multi-Sensor System, J. Hydrol., 541, 862–872, doi:10.1016/j.jhydrol.2016.07.047, 2016.

Draine, B. T. and Flatau, P. J.: Discrete-Dipole Approximation For Scattering Calculations, J. Opt. Soc. Am. A, 11(4), 1491, doi:10.1364/josaa.11.001491, 1994.

Garrett, T. J., Fallgatter, C., Shkurko, K. and Howlett, D.: Fall speed measurement and high-resolution multi-angle photography of hydrometeors in free fall, Atmos. Meas. Tech., doi:10.5194/amt-5-2625-2012, 2012.

Geer, A. J. and Baordo, F.: Improved scattering radiative transfer for frozen hydrometeors at microwave frequencies, Atmos. Meas. Tech., doi:10.5194/amt-7-1839-2014, 2014.

Gelaro, R., McCarty, W., Suárez, M. J., Todling, R., Molod, A., Takacs, L., Randles, C. A., Darmenov, A., Bosilovich, M. G., Reichle, R., Wargan, K., Coy, L., Cullather, R., Draper, C., Akella, S., Buchard, V., Conaty, A., da Silva, A. M., Gu, W., Kim, G. K., Koster, R., Lucchesi, R., Merkova, D., Nielsen, J. E., Partyka, G., Pawson, S., Putman, W., Rienecker, M., Schubert, S. D., Sienkiewicz, M. and Zhao, B.: The modern-era retrospective analysis for research and applications, version 2 (MERRA-2), J. Clim., 30(14), 5419–5454, doi:10.1175/JCLI-D-16-0758.1, 2017.

Gong, J. and Wu, D. L.: Microphysical properties of frozen particles inferred from Global Precipitation Measurement (GPM) Microwave Imager (GMI) polarimetric measurements, Atmos. Chem. Phys., 17(4), 2741–2757, doi:10.5194/acp-17-2741-2017, 2017.

Grazioli, J., Genthon, C., Boudevillain, B., Duran-Alarcon, C., Del Guasta, M., Madeleine, J. B. and Berne, A.: Measurements of precipitation in Dumont d'Urville, Adélie Land, East Antarctica, Cryosphere, doi:10.5194/tc-11-1797-2017, 2017.

https://doi.org/10.5194/acp-2020-757
Preprint. Discussion started: 30 July 2020




Honeyager, R., Liu, G. and Nowell, H.: Voronoi diagram-based spheroid model for microwave scattering of complex snow aggregates, J. Quant. Spectrosc. Radiat. Transf., 170, 28–44, doi:10.1016/j.jqsrt.2015.10.025, 2016.

Hudak, D., Rodriguez, P. and Donaldson, N.: Validation of the CloudSat precipitation occurrence algorithm using the Canadian C band radar network, J. Geophys. Res., 113, D00A07, doi:10.1029/2008JD009992, 2008.

Katsumata, M., Uyeda, H., Iwanami, K. and Liu, G.: The response of 36- and 89-GHz microwave channels to convective snow clouds over ocean: Observation and modeling, J. Appl. Meteorol., 39(12 PART 2), 2322–2335, doi:10.1175/1520-0450(2000)039<2322:troagm>2.0.co;2, 2000.

Kim, M. J., Weinman, J. A., Olson, W. S., Chang, D. E., Skofronick-Jackson, G. and Wang, J. R.: A physical model to estimate snowfall over land using AMSU-B observations, J. Geophys. Res. Atmos., doi:10.1029/2007JD008589, 2008.

Kongoli, C., Meng, H., Dong, J. and Ferraro, R.: A snowfall detection algorithm over land utilizing high-frequency passive microwave measurements—Application to ATMS, J. Geophys. Res., doi:10.1002/2014JD022427, 2015.

Kruger, A. and Krajewski, W. F.: Two-dimensional video disdrometer: A description, J. Atmos. Ocean. Technol., doi:10.1175/1520-0426(2002)019<0602:TDVDAD>2.0.CO;2, 2002.

Kulie, M. S. and Bennartz, R.: Utilizing spaceborne radars to retrieve dry Snowfall, J. Appl. Meteorol. Climatol., 48(12), 2564–2580, doi:10.1175/2009JAMC2193.1, 2009.

Kulie, M. S., Milani, L., Wood, N. B., Tushaus, S. A., Bennartz, R., L'Ecuyer, T. S. and L'Ecuyer, T. S.: A shallow cumuliform snowfall census using spaceborne radar, J. Hydrometeorol., 17(4), 1261–1279, doi:10.1175/JHM-D-15-0123.1, 2016.

Kummerow, C., Oison, W. S. and Giglio, L.: A simplified scheme for obtaining precipitation and vertical hydrometeor profiles from passive microwave sensors, IEEE Trans. Geosci. Remote Sens., doi:10.1109/36.536538, 1996.

Kummerow, C. D., Randel, D. L., Kulie, M., Wang, N. Y., Ferraro, R., Joseph Munchak,

S. and Petkovic, V.: The evolution of the goddard profiling algorithm to a fully parametric scheme, J. Atmos. Ocean. Technol., doi:10.1175/JTECH-D-15-0039.1, 2015.

Liu, G.: A fast and accurate model for microwave radiance calculations, J. Meteorol. Soc. Japan, doi:10.2151/jmsj1965.76.2_335, 1998.

Liu, G.: Approximation of Single Scattering Properties of Ice and Snow Particles for High Microwave Frequencies, J. Atmos. Sci., 61(20), 2441–2456, doi:10.1175/1520-0469(2004)061<2441:AOSSPO>2.0.CO;2, 2004.

Liu, G.: Deriving snow cloud characteristics from CloudSat observations, J. Geophys. Res. Atmos., 114(8), 1–13, doi:10.1029/2007JD009766, 2008a.

Liu, G.: A database of microwave single-scattering properties for nonspherical ice particles, Bull. Am. Meteorol. Soc., 89(10), 1563–1570, doi:10.1175/2008BAMS2486.1, 2008b.

Liu, G. and Curry, J. A.: Precipitation characteristics in Greenland-Iceland-Norwegian Seas determined by using satellite microwave data and modeling studies that require Observations Salinity satellite retrievals are the only platform from described by Schmitt cycle for tropical , , 102, 987–997, 1997.

Liu, G. and Seo, E.-K. K.: Detecting snowfall over land by satellite high-frequency microwave observations: The lack of scattering signature and a statistical approach, J. Geophys. Res. Atmos., 118(3), 1376–1387, doi:10.1002/jgrd.50172, 2013.

Liu, G. and Takeda, T.: Interesting findings on the precipitation of middle-level stratiform clouds in recent years are a banded mesoscale structure of rainfall and a showed that precipitation is initiated in high-level clouds (" seeder " clouds ) and it is enhanced in deep stra, , (October), 645–660, 1988.

Locatelli, J. D. and Hobbs, P. V.: Fall speeds and masses of solid precipitation particles, J. Geophys. Res., doi:10.1029/jc079i015p02185, 1974.

Löffler-Mang, M. and Joss, J.: An optical disdrometer for measuring size and velocity of hydrometeors, J. Atmos. Ocean. Technol., doi:10.1175/1520-0426(2000)017<0130:AODFMS>2.0.CO;2, 2000.

Marchand, R., Mace, G. G., Ackerman, T. and Stephens, G.: Hydrometeor detection using Cloudsat - An earth-orbiting 94-GHz cloud radar, J. Atmos. Ocean. Technol., 25(4), 519–533, doi:10.1175/2007JTECHA1006.1, 2008.

Meng, H., Dong, J., Ferraro, R., Yan, B., Zhao, L., Kongoli, C., Wang, N. Y. and Zavodsky, B.: A 1DVAR-based snowfall rate retrieval algorithm for passive microwave radiometers, J. Geophys. Res., 122(12), 6520–6540, doi:10.1002/2016JD026325, 2017.

Noh, Y. J., Liu, G., Seo, E. K., Wang, J. R. and Aonashi, K.: Development of a snowfall retrieval algorithm at high microwave frequencies, J. Geophys. Res. Atmos., doi:10.1029/2005JD006826, 2006.

Olson, W. S., Kummerow, C. D., Heymsfield, G. M. and Giglio, L.: A method for combined passive-active microwave retrievals of cloud and precipitation profiles, J. Appl. Meteorol., 35(10), 1763–1789, doi:10.1175/1520-0450(1996)035<1763:AMFCPM>2.0.CO;2, 1996.

RPG-FMCW: RPG-FMCW-94-SP/DP 94 GHz W-band Cloud Doppler Radar Instrument Installation, Operation and Software Guide (Version 2.10-1). [online] Available from: https://www.radiometer-physics.de/downloadftp/pub/PDF/Cloud Radar/RPG-FMCW-Instrument_Manual.pdf (Accessed 22 January 2020), 2015.

Praz, C., Roulet, Y. A. and Berne, A.: Solid hydrometeor classification and riming degree estimation from pictures collected with a Multi-Angle Snowflake Camera, Atmos. Meas. Tech., doi:10.5194/amt-10-1335-2017, 2017.

Sekhon, R. S. and Srivastava, R. C.: Doppler radar observations of drop- size distributions in a thunderstorm, J. Atmos. Sci., 28(6), 983–994, 1971.

Seo, E. K. and Liu, G.: Retrievals of cloud ice water path by combining ground cloud radar and satellite high-frequency microwave measurements near the ARM SGP site, J. Geophys. Res. D Atmos., 110(14), 1–15, doi:10.1029/2004JD005727, 2005.

Sims, E. M. and Liu, G.: A parameterization of the probability of snow-rain transition, J. Hydrometeorol., 16(4), 1466–1477, doi:10.1175/JHM-D-14-0211.1, 2015.

Skofronick-Jackson, G. and Johnson, B. T.: Surface and atmospheric contributions to

https://doi.org/10.5194/acp-2020-757
Preprint. Discussion started: 30 July 2020



passive microwave brightness temperatures for falling snow events, J. Geophys. Res. Atmos., 116(2), 1–16, doi:10.1029/2010JD014438, 2011.

Skofronick-Jackson, G., Petersen, W. A., Berg, W., Kidd, C., Stocker, E. F., Kirschbaum, D. B., Kakar, R., Braun, S. A., Huffman, G. J., Iguchi, T., Kirstetter, P. E., Kummerow, C., Meneghini, R., Oki, R., Olson, W. S., Takayabu, Y. N., Furukawa, K. and Wilheit, T.: The Global Precipitation Measurement (GPM) Mission for Science and Society, Bull. Am. Meteorol. Soc., 98(8), 1679–1695, doi:10.1175/BAMS-D-15-00306.1, 2017.

Skofronick-Jackson, G. M., Weinman, J. A., Kim, M. J. and Chang, D. E.: A physical model to determine snowfall over land by microwave radiometry, IEEE Trans. Geosci. Remote Sens., 42(5), 1047–1058, doi:10.1109/TGRS.2004.825585, 2004.

Stephens, G. L., Austin, R. T., Benedetti, A., Mitrescu, C., Vane, D. G., Boain, R. J., Durden, S. L., Mace, G. G. J., Sassen, K., Wang, Z., Illingworth, A. J., O'Connor, E. J., Rossow, W. B. and Miller, S. D.: The cloudsat mission and the A-Train: A new dimension of space-based observations of clouds and precipitation, Bull. Am. Meteorol. Soc., 83(12), 1771-1790+1742, doi:10.1175/BAMS-83-12-1771, 2002.

Tanelli, S., Durden, S. L., Im, E., Pak, K. S., Reinke, D. G., Partain, P., Haynes, J. M. and Marchand, R. T.: CloudSat's cloud profiling radar after two years in orbit: Performance, calibration, and processing, IEEE Trans. Geosci. Remote Sens., 46(11), 3560–3573, doi:10.1109/TGRS.2008.2002030, 2008.

Tang, G., Wen, Y., Gao, J., Long, D., Ma, Y., Wan, W. and Hong, Y.: Similarities and differences between three coexisting spaceborne radars in global rainfall and snowfall estimation, Water Resour. Res., 53(5), 3835–3853, doi:10.1002/2016WR019961, 2017.

Tokay, A., Wolff, D. B. and Petersen, W. A.: Evaluation of the new version of the laser-optical disdrometer, OTT parsivel, J. Atmos. Ocean. Technol., doi:10.1175/JTECH-D-13-00174.1, 2014.

Wang, Y., Liu, G., Seo, E. K. and Fu, Y.: Liquid water in snowing clouds: Implications for satellite remote sensing of snowfall, Atmos. Res., 131, 60–72, doi:10.1016/j.atmosres.2012.06.008, 2013.

https://doi.org/10.5194/acp-2020-757
Preprint. Discussion started: 30 July 2020




Wood, N. B., L'Ecuyer, T. S., Vane, D. G., Stephens, G. L. and Partain, P.: Level 2C snow profile process description and interface control document, version 0, CloudSat Proj., (D), 21 [online] Available from: http://www.cloudsat.cira.colostate.edu/ICD/2C-SNOW-PROFILE/2C-SNOW-PROFILE_PDICD_P_R04.pdf, 2013.

Yin, M. and Liu, G.: Developing an a priori database for passive microwave snow water retrievals over ocean, J. Geophys. Res. Atmos., 122(23), 12,960-12,981, doi:10.1002/2017JD027636, 2017.

Yin, M. and Liu, G.: Assessment of GPM high-frequency microwave measurements with radiative transfer simulation under snowfall conditions, Q. J. R. Meteorol. Soc., 145(721), 1603–1616, doi:10.1002/qj.3515, 2019.

Yuter, S. E. and Houze, R. A.: Three-Dimensional Kinematic and Microphysical Evolution of Florida Cumulonimbus. Part II: Frequency Distributions of Vertical Velocity, Reflectivity, and Differential Reflectivity, Mon. Weather Rev., 123(7), 1941–1963, doi:10.1175/1520-0493(1995)123<1941:tdkame>2.0.co;2, 1995.

Zhang, J., Howard, K., Langston, C., Kaney, B., Qi, Y., Tang, L., Grams, H., Wang, Y., Cocks, S., Martinaitis, S., Arthur, A., Cooper, K., Brogden, J. and Kitzmiller, D.: Multi-Radar Multi-Sensor (MRMS) Quantitative Precipitation Estimation: Initial Operating Capabilities, Bull. Am. Meteorol. Soc., 97(4), 621–638, doi:10.1175/BAMS-D-14-00174.1, 2016.

https://doi.org/10.5194/acp-2020-757
Preprint. Discussion started: 30 July 2020

Atmospheric Chemistry and Physics
Discussions

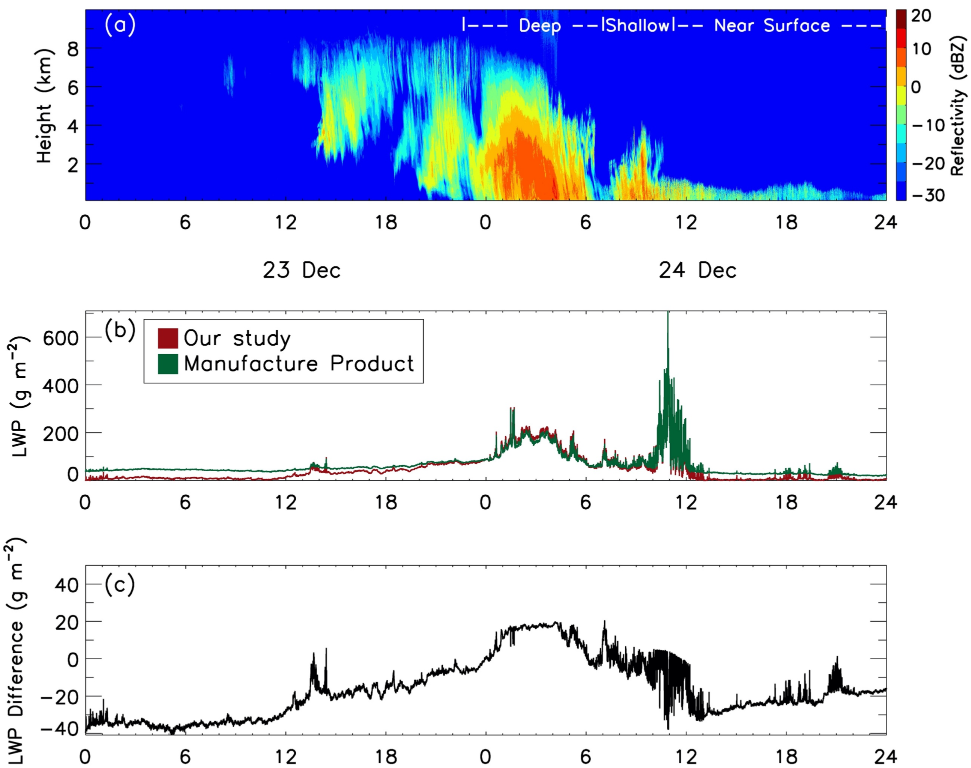


Fig.1 (a) Radar reflectivity, (b) two liquid water path retrievals and (c) their differences (LWP of our study plus manufacture product) for observations during 23 and 24 December 2017. In the top panel, cloud types as defined in the text are also indicated.

https://doi.org/10.5194/acp-2020-757
Preprint. Discussion started: 30 July 2020



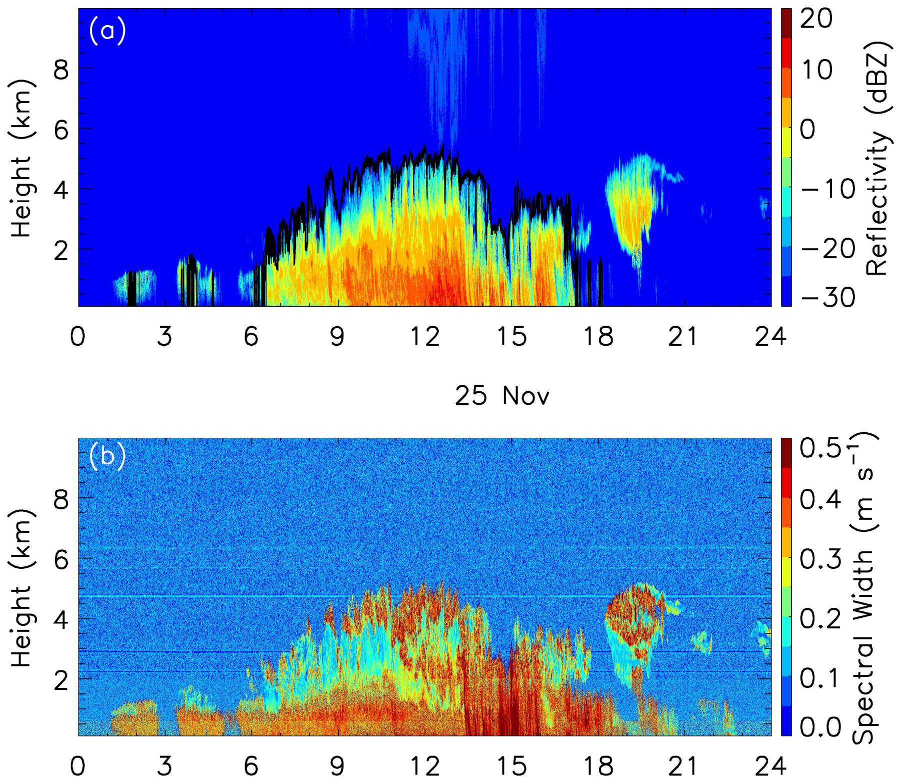


Fig.2 Height-time cross section of (a) radar reflectivity and (b) Doppler spectral width for observations on 25 November 2017. The cloud top for snowing clouds (surface radar reflectivity greater than -20 dBZ) is also shown in the top panel.

https://doi.org/10.5194/acp-2020-757
Preprint. Discussion started: 30 July 2020

Atmospheric Chemistry and Physics
Discussions

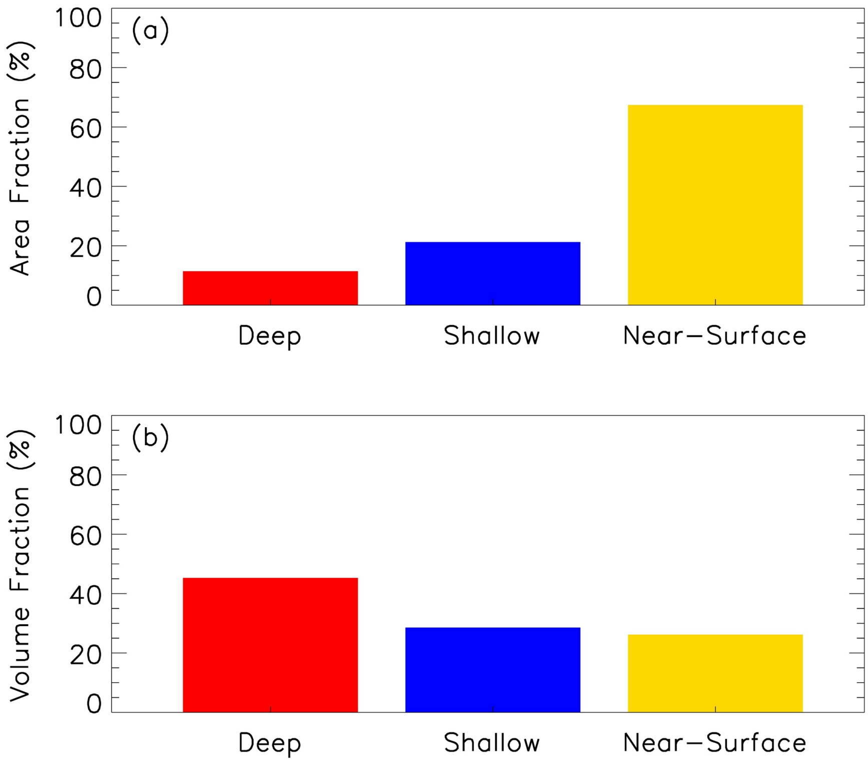


Fig.3 (a) Area and (b) volume fractions of the 3 types of snowing clouds observed during the 2017-18 winter season.

https://doi.org/10.5194/acp-2020-757
Preprint. Discussion started: 30 July 2020



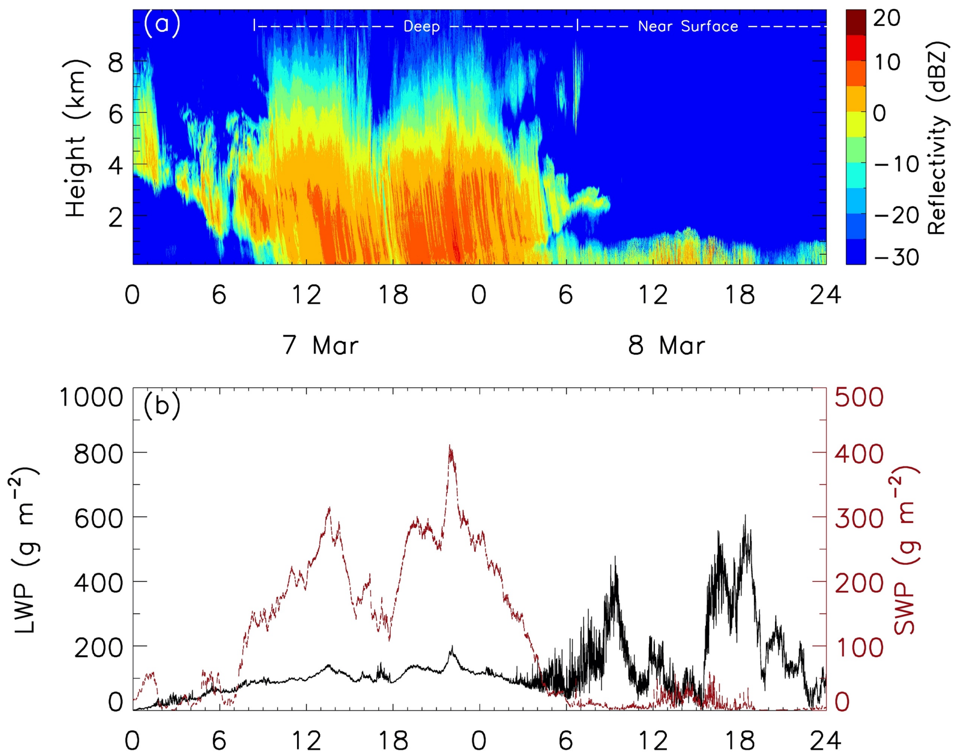


Fig.4 (a) Height-time cross section of radar reflectivity and (b) time series of liquid water path (LWP, black) and snow water path (SWP, red) for observations on 7 and 8 March 2018.

https://doi.org/10.5194/acp-2020-757
Preprint. Discussion started: 30 July 2020

Atmospheric Chemistry and Physics
Discussions

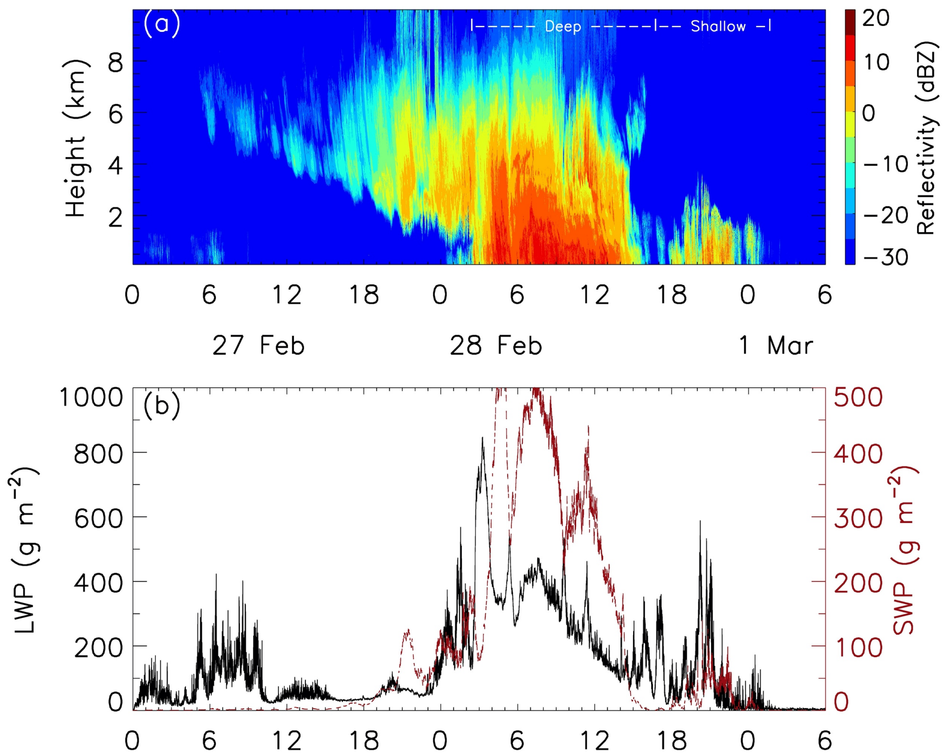


Fig.5 (a) Height-time cross section of radar reflectivity and (b) time series of liquid water path (LWP, black) and snow water path (SWP, red) for observations from 27 February through 1 March 2018.

https://doi.org/10.5194/acp-2020-757
Preprint. Discussion started: 30 July 2020

Atmospheric Chemistry and Physics Discussions
Open Access

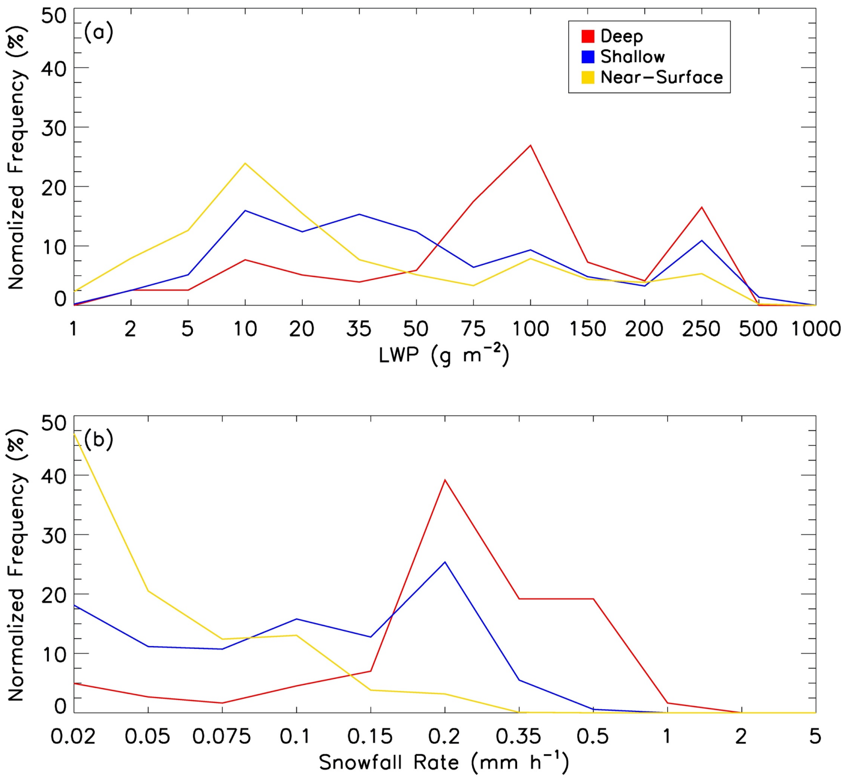


Fig.6 Frequency distribution of (a) liquid water path and (b) snowfall rate at surface derived from all observed snowfall data during the 2017-18 winter. The frequency values are normalized so that the sum of their values at all bins is 100%.

https://doi.org/10.5194/acp-2020-757
Preprint. Discussion started: 30 July 2020


Atmospheric Chemistry and Physics
Discussions

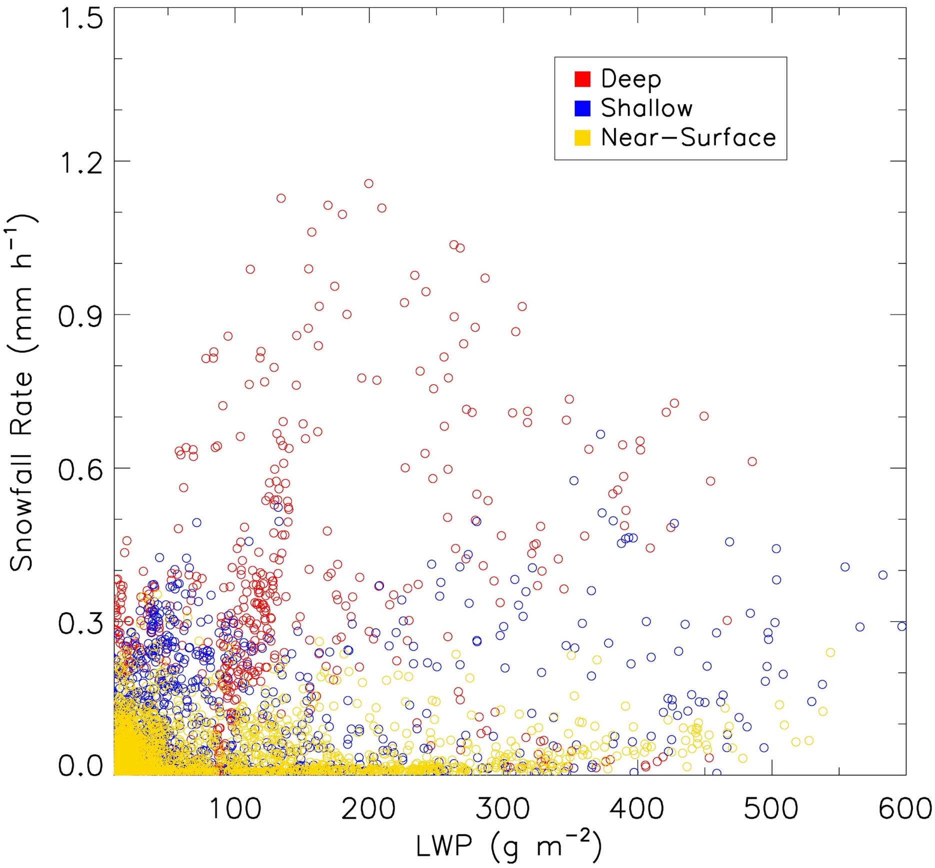


Fig.7 Scatterplot of liquid water path and surface snowfall rate. Each point is an average of 5-minute data. All observed data during the 2017-18 winter are included.

https://doi.org/10.5194/acp-2020-757
Preprint. Discussion started: 30 July 2020




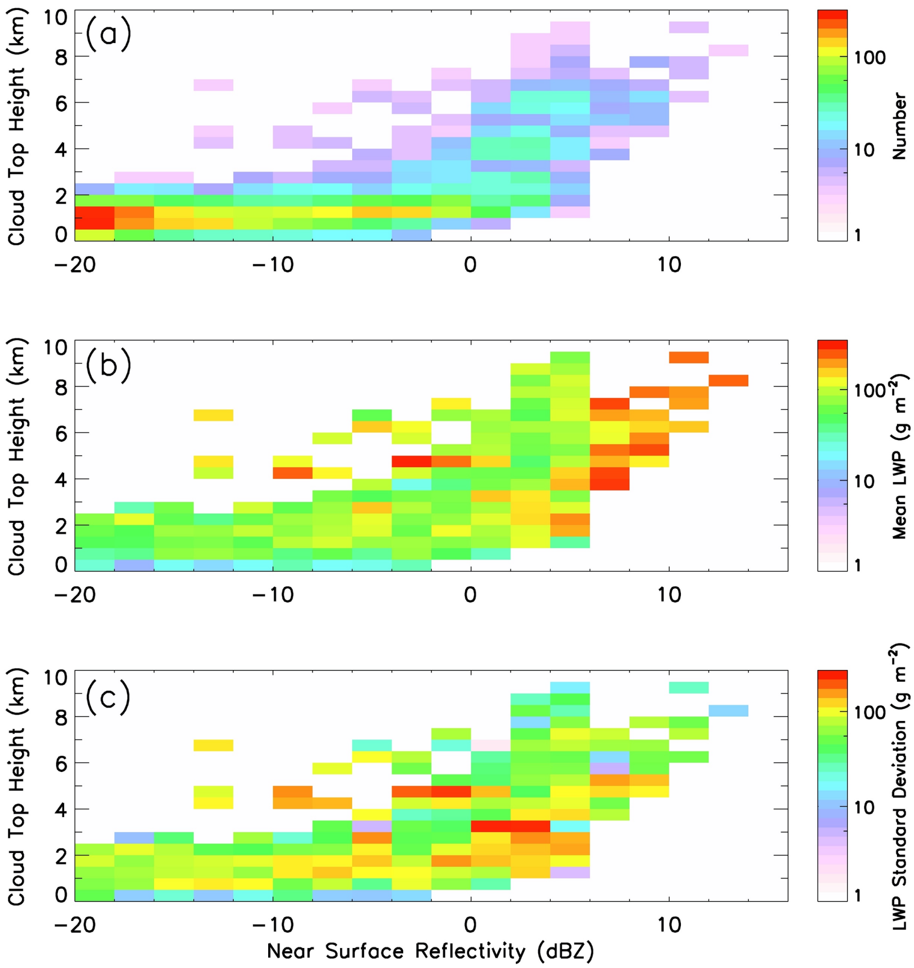


Fig.8 Two-dimensional distributions of (a) number of occurrences, (b) liquid water path and (c) standard deviation of liquid water path as a function of near surface radar reflectivity and cloud top height. All observed data during the 2017-18 winter are used in calculate the distributions.

https://doi.org/10.5194/acp-2020-757
Preprint. Discussion started: 30 July 2020




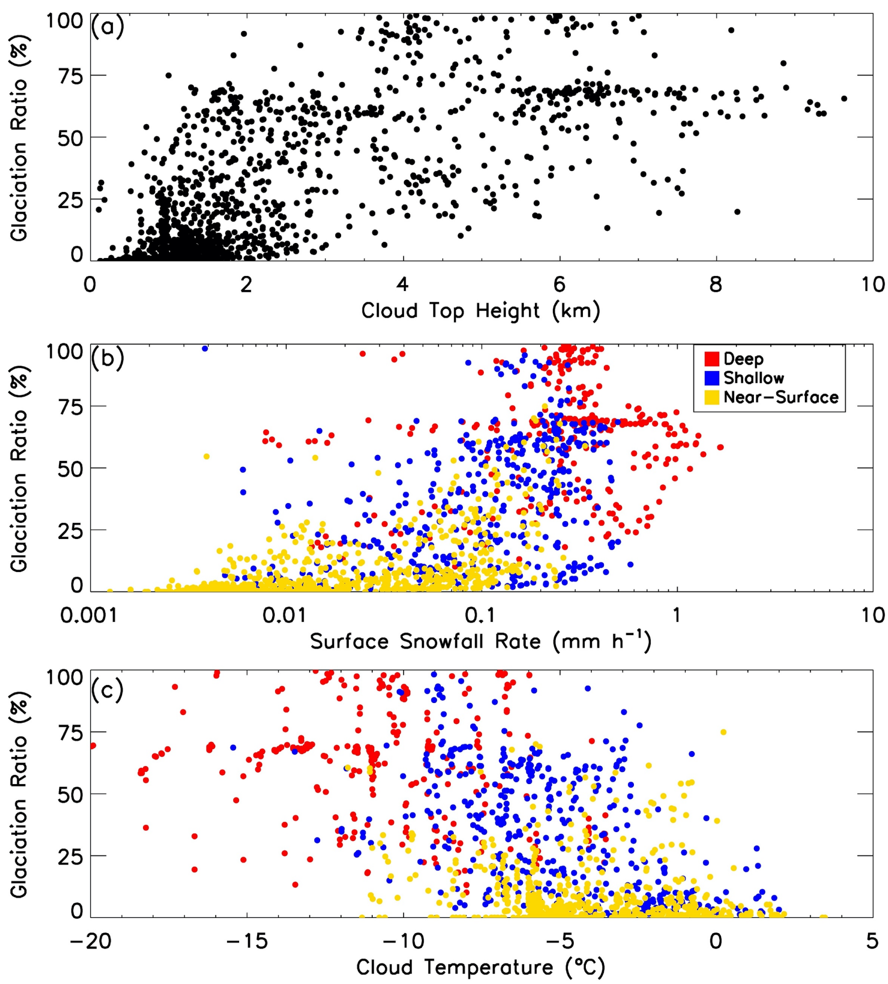


Fig.9 Scatterplot of glaciation ratio (see definition in the text) with (a) cloud top height, (b) surface snowfall rate and (c) cloud temperature based on 5-minute averages of all observational data of snowing clouds in the 2017-18 winter.

https://doi.org/10.5194/acp-2020-757
Preprint. Discussion started: 30 July 2020

Atmospheric Chemistry and Physics
Discussions

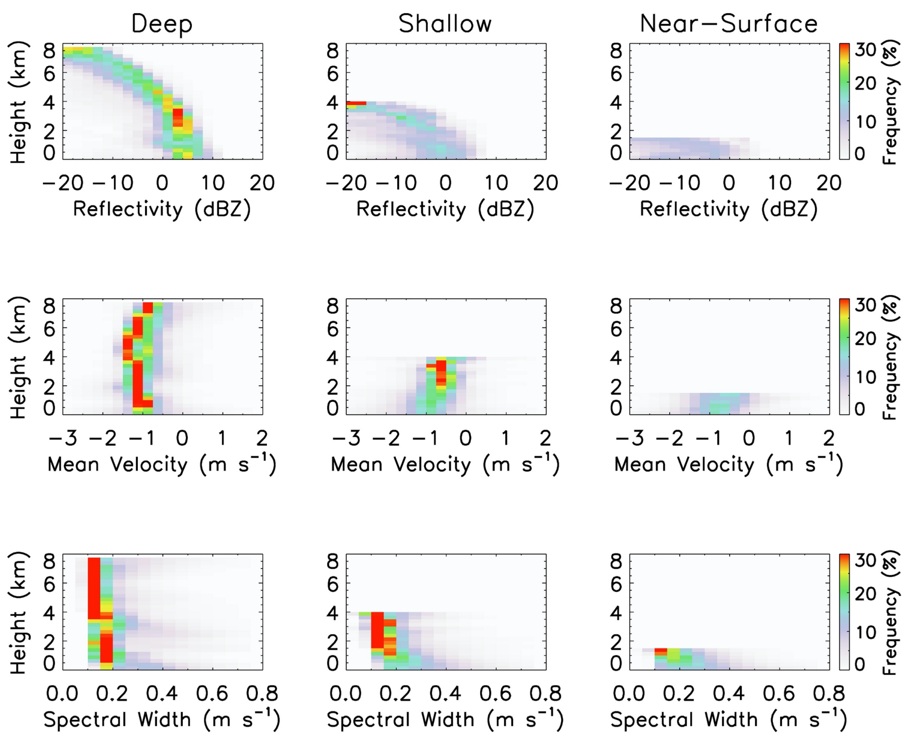


Fig.10 Contoured frequency by altitude diagram (CFADs) for radar reflectivity (top), mean Doppler velocity (middle) and Doppler spectral width (bottom) for deep (left), shallow (middle) and near-surface (right) snowing clouds. The frequency values are calculated in such a way that the sum of all frequency values at each altitude is 100%. All observed data from the 2017-18 winter are used.

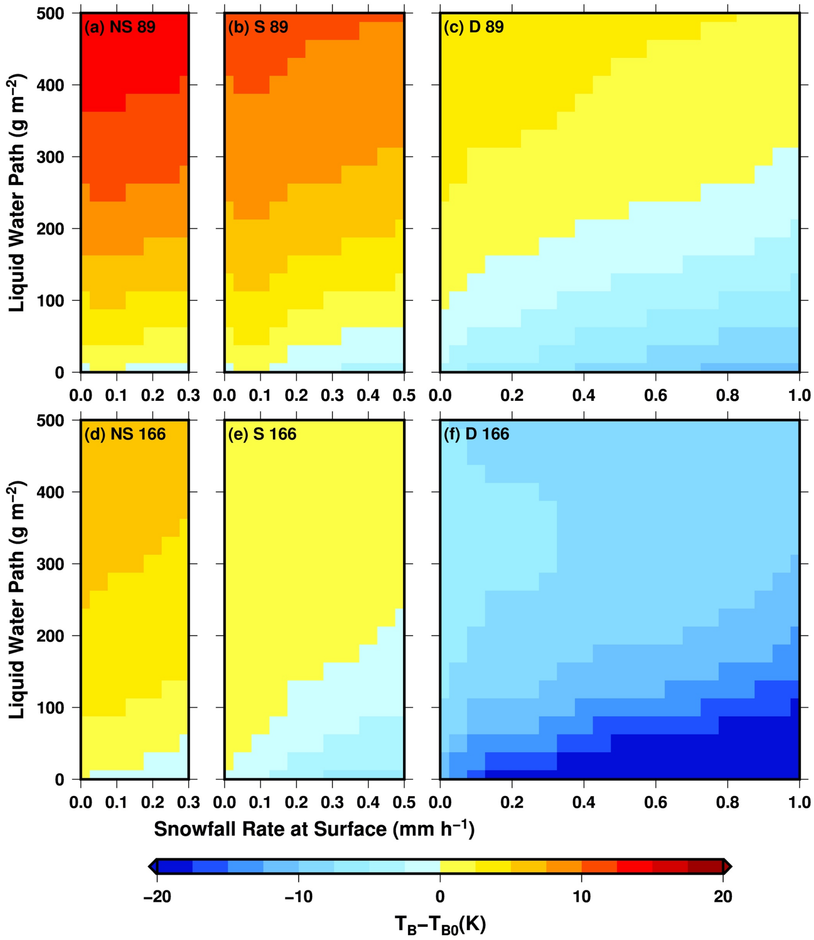


Fig.11 Simulated brightness temperature change (relative to clear-sky) at GMI 89 GHz (top) and 166 GHz (bottom) for near-surface (left), shallow (middle) and deep (right) snowing clouds. The change is relative to values at clear-sky.

https://doi.org/10.5194/acp-2020-757
Preprint. Discussion started: 30 July 2020


Atmospheric Chemistry and Physics
Discussions

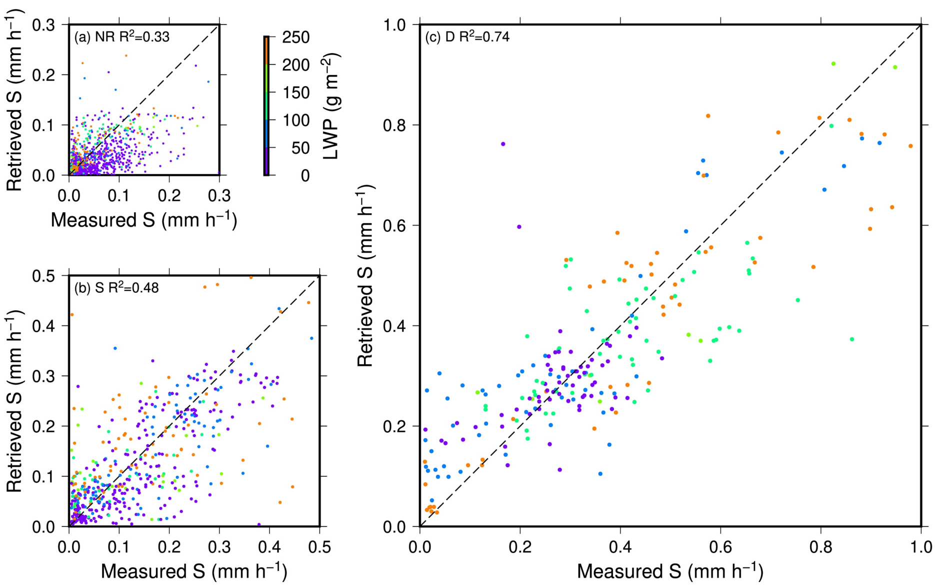


Fig.12 Scatterplot of "measured" versus "retrieved" snowfall rate for (a) near-surface, (b) shallow and (c) deep snowing clouds over land. Color of the points indicates liquid water path associated with the case. Correlation is indicated by $R^2$ in each diagram.

https://doi.org/10.5194/acp-2020-757
Preprint. Discussion started: 30 July 2020


Atmospheric Chemistry and Physics Discussions

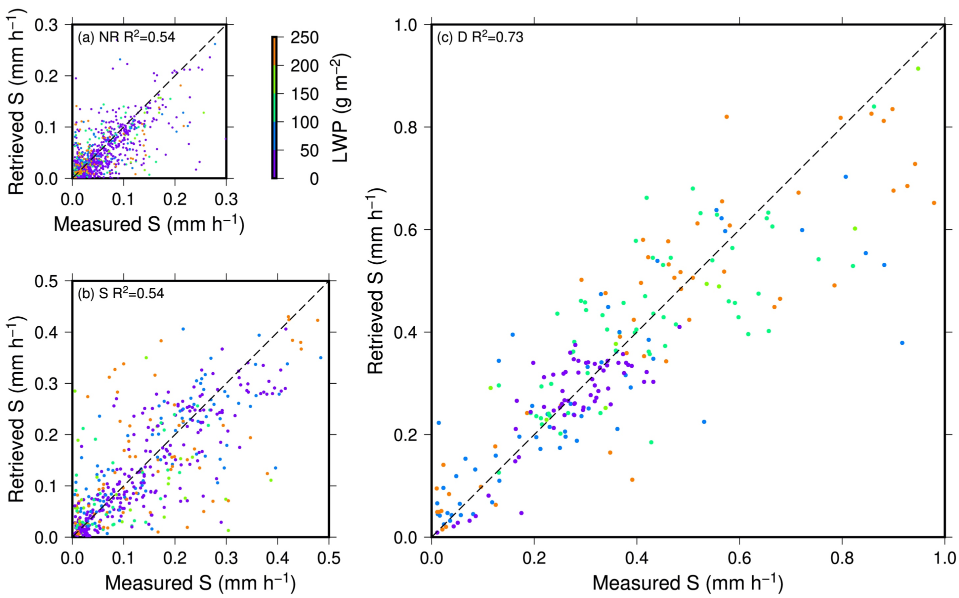


Fig.13 Scatterplot of "measured" versus "retrieved" snowfall rate for (a) near-surface, (b) shallow and (c) deep snowing clouds over ocean. Color of the points indicates liquid water path associated with the case. Correlation is indicated by $R^2$ in each diagram.

https://doi.org/10.5194/acp-2020-757
Preprint. Discussion started: 30 July 2020




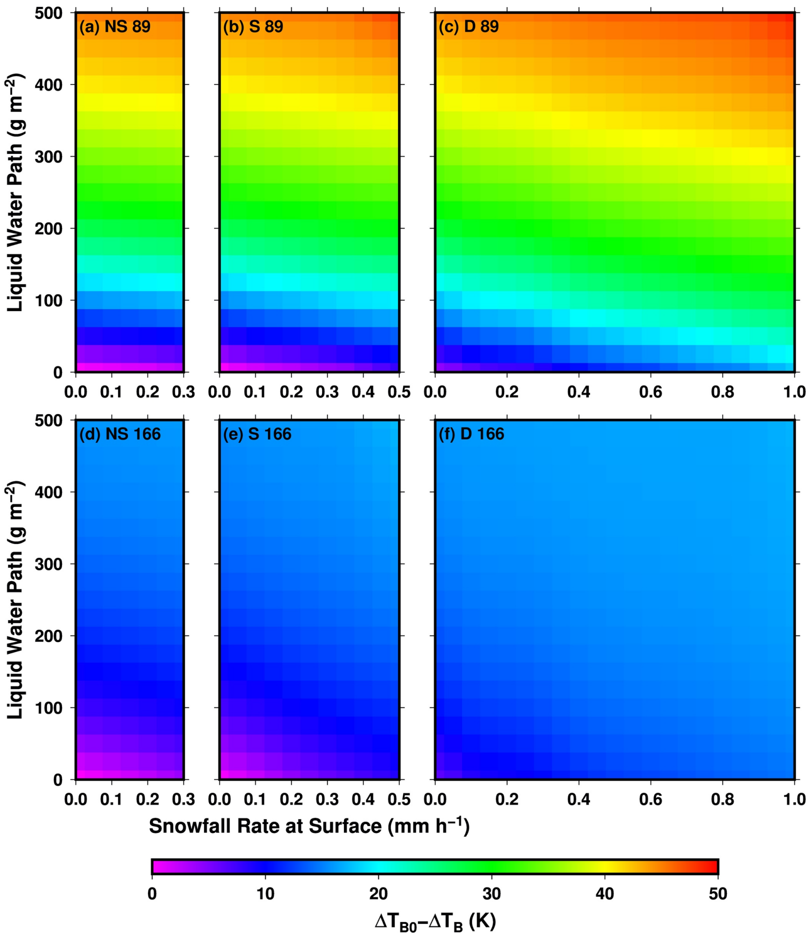


Fig.14 Simulated change of depolarization for GMI 89 GHz (top) and 166 GHz (bottom) for near-surface (left), shallow (middle) and deep (right) snowing clouds over ocean. Depolarization is the brightness temperature difference between vertical and horizontal polarizations. The change is relative to values at clear-sky.